Journal of Advanced Scientific Research

Available online through http://www.sciensage.info

ISSN
0976-9595
Research Article

BIOLOGICAL ACTIVITY OF FLUORESCENT COPPER COMPLEX: SYNTHESIS, CRYSTAL STRUCTURE, DFT AND PROTEIN BINDING STUDY

Gobinda Prasad Sahoo[1], Akhil Pandey[2], Madhumita Hazra[3], Animesh Patra*[1]

[1]*Postgraduate Department of Chemistry, Midnapore College, Midnapore, West Bengal, India*

[2]*Department of Botany, Midnapore college, Midnapore, West Bengal, India*

[3]*Department of Chemistry, PRMS Mahabidyalaya, Jamboni, Bankura, West Bengal, India*

**Corresponding author: animeshpatrarl@yahoo.com, animeshpatramc@gmail.com*

ABSTRACT

Synthesis of square planar copper (II) complex with formula [Cu $(DMAP)_2(NCS)_2$] (**1**) (DMAP =N,N-dimethyl-4 aminopyridine) was done and characterized by various spectroscopic and single-crystal X-ray diffraction study. Complex 1 crystallizes in the monoclinic space group, P 21/c, with cell dimensions a = 6.066(2), b = 10.702(4), c = 14.561(5) Å, a = 90 b = 93.11(2) and c = 90. The electron transfer mechanism of copper (II) complex was measured by cyclic voltammetry and indicate copper (II) complex is the Cu(II)/Cu(I) couple. The electronic structure and spectral properties of the complex-1 has been explained by density functional theory (DFT) and time dependent density functional theory (TDDFT) calculations. *In-vitro*, human serum albumin (HSA) binding was also carried out using absorption and fluorescence technique, which showed considerable binding affinities of the complex with HSA. Again we report the synthesis of copper complex-HSA microcrystals. The complex has been screened for antimicrobial activity by agar disk diffusion and minimum inhibitory concentration (MIC) strain against some pathogenic bacteria.

Keywords: Copper complex, Crystal structure, HSA binding, Antibacterial activity.

1. INTRODUCTION

Copper is now recognized as an essential trace element and third most abundant in humans, which is present in the liver [1], and brain [2] with the highest concentrations in low levels in comparison to other organs. The general bioavailability and metabolic fate of dietary Cu in humans are well understood. However, it is toxic at higher concentration, for example, the accumulation of Cu^{2+} in the liver and kidney may cause Wilson's disease [3], dyslexia, hypoglycemia and infant liver damage [4-6], gastrointestinal disease. Cu(II) complexes displays a variety of coordination numbers and geometries forms with different kinds of applications. Geometries of such types of Cu(II) complexes are octahedral, square pyramidal or trigonal bipyramidal and tetrahedral or square planar [7].

Human serum albumin (HSA) is the main components in plasma protein for humans. It is constructed by three structurally homologous domains (I, II and III), each subdomains containing A and B. Ligands containing heterocyclic and aromatic compounds are bind hydro-phobic pockets in subdomains IIA and IIIA, described as site I and site II [8]. The most significant functions of serum albumins are to control the osmotic pressure [9] and pH of blood and to transport an extensive variety of endogenous and exogenous com-pounds, as well as drugs and nutrients, mostly through the formation of noncovalent complexes at specific binding sites [10]. HSA frequently increases the noticeable solubility of hydrophobic drugs in plasma and modulates their delivery to cell *in vivo* and *in vitro*. Thus, it is essential to study the interactions of drugs with serum albumin, which determines the pharmacology and pharma-codynamics of drugs.

In the present work, we report the interaction between copper complex and HSA under physiological conditions by spectroscopic methods. Meanwhile the optical waveguide properties of copper complex-HSA microstructures measured by optical and fluorescence microscopy study. Since the compound is strongly bound with protein, we investigated the antibacterial activity by agar disk diffusion method and minimum inhibitory concentration (MIC) strain against two Gram-positive bacteria *(Bacillus cereus and Staphylococcus aureus)* and two Gram-negative bacteria (*Vibrio cholera, E. coli*).

2. MATERIAL AND METHODS

2.1. Reagents and Instruments

Chemicals and reagents are used in this report were obtained from commercial sources and used as received. Doubly distilled solvents are used for chemical reactions. Perkin Elmer model 2400 elemental analyzer was used for the elemental (C, H, N) analyses. Varian atomic absorption spectrophotometer (AAS) model-AA55B, GTA using graphite furnace applied for copper analysis. Shimadzu UV-1800 spectrophotometer and Fluorimeter (Hitachi-7000) are used for electronic absorption spectra and fluorescence spectra respectively. Perkin-Elmer FT-IR model RX1 spectro-meter was used for IR measurement. The magnetic susceptibility was measured by using a vibrating sample magnetometer PAR 155 model at room temperature. Systronics conductivity meter 304 model used for molar conductances ($_M$) mesurement. Electrochemical measure-ments were performed using computer-controlled CH-Instruments (Model No- CHI620D). Optical micros-copy images were taken using an Nikon Eclipse LV100POL upright microscope equipped with a 12V-50W halogen lamp.

2.2. Synthesis of $[Cu(DMAP)_2(NCS)_2]$ (1)

To prepare the copper (II) complex, a general process was followed as described below, using copper (II) acetate and the DMAP in (1:2) molar ratio. A methanolic solution of DMAP (2.0 mmol) was mixed with 1.0 mmol of copper (II) acetate with stirring condition and the mixture was stirred for 2 h. After that an aqueous solution of ammonium thiocyanate (0.154g, 2 mmol) was added to this clear solution with nonstop stirring for 30 min. The solid product was collected and dried. A deep green single crystal, suitable for X-ray diffraction, was obtained after few weeks by slow evaporation of a DMF solution of this green compound in open atmosphere.

Complex **1:** $C_{16}H_{20}CuN_6S_2$: Yield 80-85%; Anal.Found; C,45.28; H, 4.62; N, 19.81; Cu, 14.97; Calc: C, 45.12; H, 4.56; N, 19.62; Cu, 14.51. IR data (KBr, cm^{-1}): νSCN, 2096; $\nu_{C=N}$, 1618; $\nu_{N-CH3,}$ 1227. m.p. 210±1°C. Magnetic moment (μ, B.M.): 1.82. Conductivity (Λo, $ohm^{-1} cm^2 mol^{-1}$) in acetonitrile: 134.

2.3. Synthesis of copper complex-HSA microrods

The synthesis of copper complex-HSA microrods as described below, 6μM HSA and 20μM compound are dissolved in 80 μL of phosphate buffer solution of pH 7.4. At room temperature, the mixture was incubating for 1h with shaking. Incubation was followed with centrifuged at1000 rpm for about 40 min, which allows the exclusion of any unbound protein molecule. In buffer (pH 7.4), negative ions of HSA molecules attached with copper(II) complex by columbic interaction and weak non-covalent interaction produces microrods.

2.4. Theoretical methodology

All molecular calculations were performed in the gas phase using Density Functional Theory (DFT) using the hybrid functional B3LYP (Becke three-parameter Lee-Yang-Parr) exchange correlation functional with 6-31G basis set. The lanL2TZ(f) basis set with useful core potential was applied for the Cu atom [11]. The vibrational frequency calculations were observed to make sure that the optimized geometries represent the local minima and that there is only positive eigen values. Vertical electronic excitations based on B3LYP optimized geometries were computed using the time dependent density functional theory (TDDFT) formalism in acetonitrile using a conductor-like polarizable continuum model (CPCM) [12, 13]. All calculations were carried out using the GAUSSIAN 09 program package with the aid of the Gauss View visualization program [14].

2.5. Crystallographic analysis

The Single X-ray crystal structure study of copper complex was carried out by collecting the diffraction data using MoKα radiation (λ= 0.71073 Å) at 296 K. The data were corrected for Lorentz and polarization effects and empirical absorption corrections were applied using SADABS from Bruker. The structure was solved by direct methods using SIR-9211 and refined by full matrix least squares refinement process based on F2, using SHELXL-2013 [15]. All non-hydrogen atoms were developed anisotropically. All calculations were performed using the Wingx package [16].

2.6. Protein binding experiments

Copper complex binding with human serum albumin was performed by fluorimetric titration. The aqueous solution of protein was titrated by addition of the proper concentration of copper (II) complex solution (to give a final concentration of 4.8×10^{-6} mol L^{-1}). For every addition, the solution mixture was shaken and allowed to stand for 30 minute and then the

fluorescence intensities were measured with an excitation wavelength of 278 nm.

2.7. Antimicrobial Screening

The DMAP and synthesized compound were used for their antibacterial activities *in vitro* against two gram negative (*Vibrio cholera, E. coli*) and two gram positive (*Bacillus cereus, Staphyloccus aureus)* pathogenic bacteria. The test compound and standard antibiotics are dissolved in DMF solvent. The compound and standards were added to the agar plates and incubation of the plates was done at 37°C for 24 hours [17]. The inhibition zone was measured, and then compared to the standard antibiotics. Finally minimal inhibitory concentrations (MIC) of the compounds were determined by the agar diffusion assay.

3. RESULTS AND DISCUSSION

3.1. Synthesis and X-ray crystal structure of complex-1

The compound was prepared by using a methanolic solution of DMAP with copper acetate in 2:1 mole ratio then ammonium thiocyanide was added at stirring condition. The copper compound was characterized by physicochemical and spectroscopic tools and finally the structure was established by single crystal X-ray crystallography. The complex conductivity measurement in acetonitrile shows conductance values of 134 (Λo, ohm^{-1} cm^2 mol^{-1}) suggest that complex exists in solution as non-electrolytes [18]. The molecular view of compound with atom labelling scheme is shown in Fig. 1. The crystallographic data is presented in Table 1, bond length and bond angle are tabulated in Table 2. The copper complex, Cu is bound to two N-atom of DMAP and two N-atom of thiocyanate ion. The Cu-$N_{thiocyanate}$ {1.953(4) Å} is slightly shorter than the Cu-N_{DMAP} {2.022(4)Å} distance. The sum of the bond angles around copper (II) is 360°, representing square-planar geometry around the copper (II) centre.

3.2. Spectral characterization

The IR spectrum of the complex **1** shows intense band at 1618 cm^{-1} and 1227 cm^{-1} assigned to C=N and N-CH_3 stretching frequency, respectively and the characteristic strong band at 2096 cm^{-1} indicate the presence of the N-bonded SCN group [19].

The electronic spectrum of the complex in acetonitrile was recorded in the range 200-800 nm. The presence of intense absorption bands at short wavelengths, around 362 nm, may be due to ligand to metal ion charge transfer bands (LMCT). The bands at 283, 256 nm may be assigned to intra ligand charge transfer transitions. The observed square planar geometries around the copper (II) centres confirms by using the presence of these UV-Vis spectral bands [20].

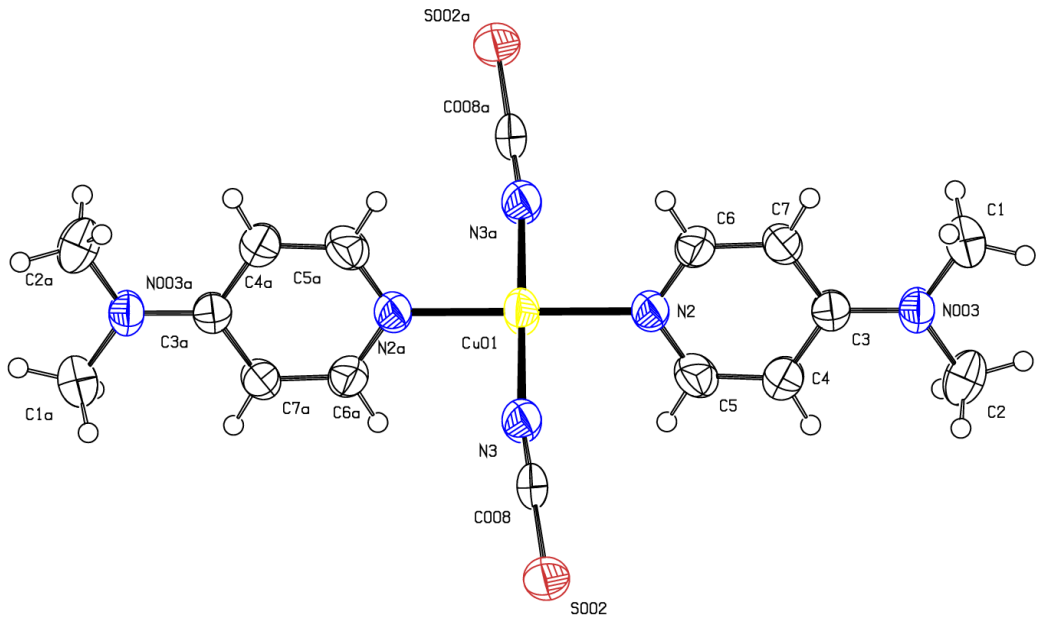

Fig. 1: ORTEP plot of $[Cu(DMAP)_2(SCN)_2]$ with 50% ellipsoidal probability

Table 1: Crystallographic data for [Cu(DMAP)$_2$ (SCN)$_2$] (1)

Structure	BEP
Empirical formula	C_{16} H_{20} Cu N_6 S_2
Formula weight	424.07
Temperature (K)	296(2)
Wavelength (°A)	0.71073
Crystal system	Monoclinic
Space group	P 21/c
Volume (°A^3)	943.9(6)
a, b, c (°A)	6.066(2), 10.702(4), 14.561(5)
α, β, γ (°)	90, 93.11(2), 90
F(000)	438
Absorption coefficient (mm^{-1})	1.390
Z	2
ρ_{calc} (g/cm^3)	1.492
θ range(deg)	2.363-22.431
Max. and min. transmission	0.991and 0.711
*R*1 [$I > 2.0\ \sigma(I)$]	0.0335, 0.1276
wR2	0.0947, 1.000
Collected refinement	1219
Goodness-of-fit	1.000

Table 2: X-ray and calculated (DFT/B3LYP) bond distances (Å) and angles (^{0}) of [Cu(DMAP)$_2$(SCN)$_2$] (1)

Bond Length(A^0)	Single crystal XRD data	[B3LYP/ 631G]
Cu(1)- N(3)	1.953(4)	1.956
Cu(1)- N(2)	2.022(4)	2.046
N(3)- C(3)	1.350(5)	1.362
N(3)- C(1)	1.442(6)	1.449
N(3)- C(2)	1.450(5)	1.462
N(2) –C(6)	1.334(5)	1. 347
N(2)- C(5)	1.342(6)	1.352
S(2) –C(8)	1.641(5)	1.651
Bond Angle(^{0})		
N(3)- Cu(1)- N(3)	180.0	180.0
N(3)- Cu(1)- N(2)	89.67(15)	90.326
N(2)- Cu(1)- N(2)	180.0	180.0
C(3)- N(2)- C(2)	121.8(4)	121.86
C(6)- N(2)- Cu(1)	122.6(3)	122.63
C(5)- N(2)- Cu(1)	121.9(3)	122.63
C(3)- N(3)- C(1)	121.6(4)	121.77

3.3. TDDFT calculation and electronic spectra

The frontier orbitals of HOMO and LUMO of the ligand are given in Fig. 2. The HOMO orbital of compound is distributed on aromatic and thiocyanate group, whereas the LUMO orbital charge distributed on pyridine group through copper [21]. The HOMO-LUMO gap is found to be 0.15968 eV, indicates requires small excitation energy. The optimized geometric parameters such as bond lengths and bond angles are listed in Table 2 along with single crystal X-ray data. As seen there was minor variations from experimental data are observed in optimized bond lengths and bond angles. These differences are due to the theoretical calculations belong to isolated molecule in gaseous phase while the experimental results belongs to molecule in solid state.

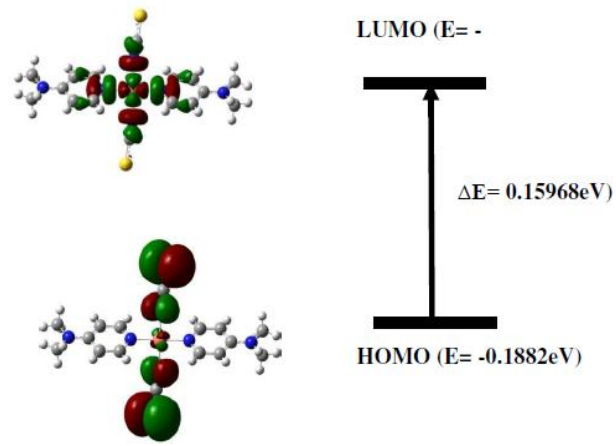

Fig. 2: HOMO and LUMO orbitals of copper complex 1 obtained from DFT

To simulate the experimental electronic spectra of the complex TDDFT calculations have been performed in acetonitrile given in Table 3. To get deep nearby into the electronic transitions, TDDFT calculation on the optimized geometry of the complex has been performed. The strong peak at 362 nm has LMCT transition and in addition, the other transition at 283 and 256 nm have mixed LMCT and ILCT character.

3.4. Electrochemistry

The electrochemical studies of the copper (II) complex was illustrated by cyclic voltammetry using a Pt-disk working electrode and a Pt-wire supporting electrode in dimethyl formamide using [*n*-Bu_4N]ClO_4 (0.1 M) as the supporting electrolyte. The cyclic voltammograms exhibit quasi-reversible transfer process with a reduction peak at E_{pc} = 0.1271V with a corresponding oxidation peak at E_{pa} = 0.4773V for copper complex at a scan rate interval 50-400 mV s^{-1} [22]. This electrode potential data indicates copper (II) complex is the Cu(II)/Cu(I) couple given in Fig. 3. The ratio of cathodic to anodic peak height was less than one. On the other hand, the peak current increases with the increase

of the square root of scan rates. From these data indicates the redox couple is interconnected to a quasi-reversible one-electron transfer route controlled by diffusion.

Table 3: Vertical excitation energies (Eex), oscillator strengths (f), and Key transitions obtained from TDDFT calculations of Cu-complex 1

$E_{excitation}$(eV)	$\lambda_{excitation}$(nm)	Osc. Strength(f)	Key transition	CI	λ_{exp}(nm)
2.1580	574.52	0.000	HOMO-2→LUMO	0.68906	362
2.4361	508.94	0.000	HOMO→LUMO	0.31135	
2.4570	504.61	0.000	HOMO-9→LUMO	0.53918	
2.8599	433.52	0.0019	HOMO-1→LUMO	0.99262	
2.9544	419.67	0.000	HOMO →LUMO	0.74539	
3.0165	411.02	0.0226	HOMO-4→LUMO	0.99454	
3.1408	394.75	0.0001	HOMO-5→LUMO	0.99473	
3.4590	358.44	0.000	HOMO-2→LUMO	0.72335	
3.5612	348.15	0.000	HOMO-3→LUMO	0.70396	
3.8653	296	0.000	HOMO-3→LUMO	0.70143	283
4.1845	288	0.001	HOMO-3→LUMO+1	0.6874	
4.5846	258	0.000	HOMO-2→LUMO	0.6438	256

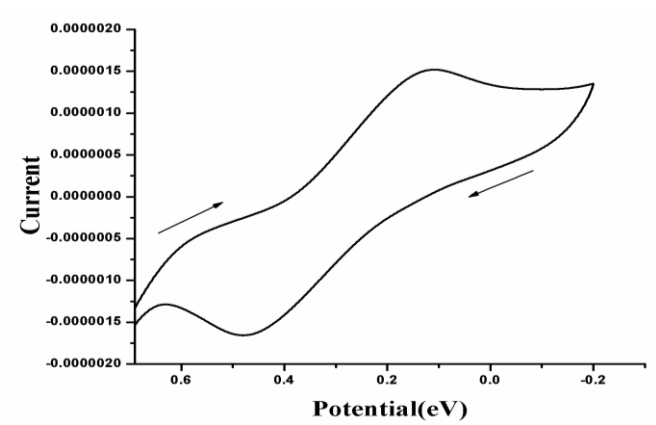

Fig. 3: Cyclic voltammogram of complex 1 in DMF

3.5. Proteins-HSA binding experiments

3.5.1. Absorption characteristics of HSA-Cu (II) complex 1

From absorption spectral study we saw that absorption of HSA increases while increasing the concentration of complex. The observation shows ground state complex formation [23]. For dynamic quenching there is no significant change in spectrum but in our experiment change in spectrum in presence of different concentration due to static quenching given in Fig. 4. Thus calculated apparent association constant (K_{app}) from the Benesi-Hildebrand equation [24].

$$1/(A_{obs} - A_0) = 1/(A_c - A_0) + 1/K_{app}(A_c - A_0)[comp]$$

Where, A_{obs} is the observed absorbance of the solution containing different concentrations of the complex at 278 nm, A_0 and Ac are the absorbances of HSA and the complex at 278 nm, respectively, and K_{app} represents the apparent association constant. The increase of absorbance at 278 nm was due to adsorption of the surface complex, based on the linear relationship between $1/(A_{obs} - A_0)$ *vs* reciprocal concentration of the complex with a slope equal to $1/K_{app}(A_c - A_0)$ and an intercept equal to $1/(A_c - A_0)$. The value of the apparent association constant (K_{app}) of HSA determined from this plot and the values were 4.26×10^4 M^{-1} (R = 0.9648). All the plots represent a good linear relationship.

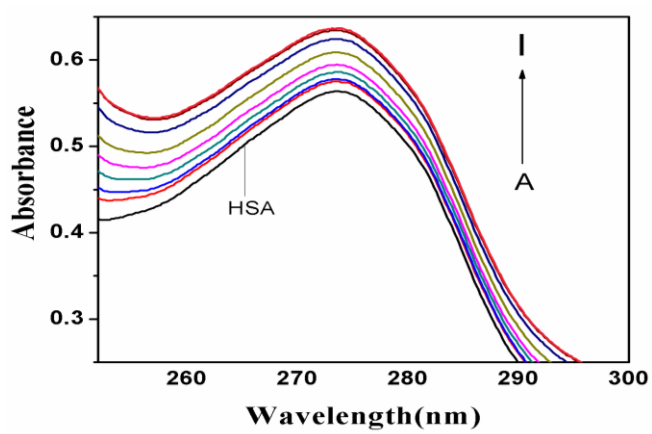

The concentration of complex varied from (A) 0.0 to (I) 3.28 × 10^{-6} ML^{-1}. Arrow indicates an increase in the concentration of complex.

Fig. 4: Electronic spectral titration of complex 1 with HSA in the presence of phosphate buffer, pH 7.4

3.5.2. *Fluorescence quenching of HSA by the Cu (II) complex 1*

The fluorescence property of protein mainly originates from the presence of tryptophan, tyrosine and phenylalanine residues. When it interacts with other compounds, its intrinsic fluorescence often changes with the ligand's concentration. Therefore, fluorescence can be regarded as a technique for study the mechanism of interactions among the ligands and proteins [25]. The fluorescence of HSA is quenched by complex-1 as seen in Fig. 5.

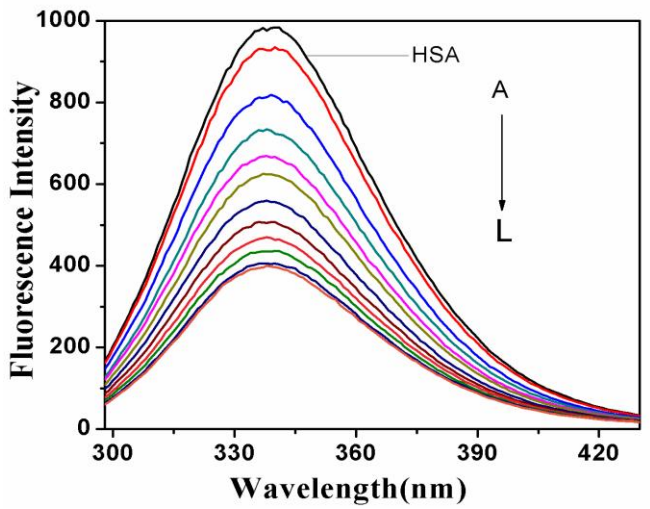

The concentration of complex varied from (A) 0.0 to (L) 3.28 × 10^{-6} ML^{-1}. Arrow indicates an increase in the concentration of complex.

Fig. 5: Change in fluorescence spectra of complex 1 with HSA, excited at 278 nm in the presence of phosphate buffer, pH 7.4.

Additionally, a little blue shift of fluorescence peak was observed with increasing complex concentration, which suggests that the fluorescence chromospheres of HSA was placed in a more hydrophobic environment after the addition of copper complex-1. The fluorescence quenching is described by the Stern–Volmer relation [26]

$$F_0/F = 1 + K_{sv}[Q]$$

Where, F_0 and F represent the fluorescence intensities in absence and presence of quencher respectively. K_{sv} is a linear Stern-Volmer quenching constant, Q is the concentration of quencher [27]. The K_{sv} value evaluated from the plot of F_0/F *versus* [Q] and the Ksv is 3.60 × 10^5 M^{-1} (R=0.9789). The Stern-Volmer plot represents (Fig. 6) a good linear relationship and demonstrating a strong affinity of the copper (II) complex to HSA.

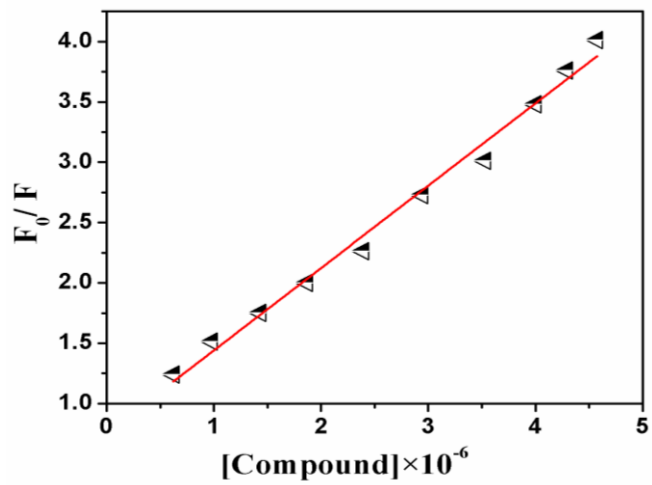

Fig. 6: Plot of Fo/F against [Compound] in case of fluorescence quenching of HSA in phosphate buffer, pH 7.4.

3.6. Analysis of binding constant and binding Site

Number of binding sites can be considered from fluorescence titration data using the subsequent equation [28]

$$\log [(F_0 - F)/F] = \log K_b + n\log[Q]$$

K_b and n is the binding constant and binding site of Cu (II) complex. From the experimental results, the linear fitting plots of log $[(F_0 - F)/F]$ versus log[Q] can be observed. The corresponding K_b (= 3.28×10^5) and n (= 0.9852) values, estimated from the slopes and intercepts of the linear plots, correspondingly. The number of binding sites n is roughly equals 1, signifying that there is one binding site (static or dynamic) in HSA for complex-1 for the period of their interaction.

3.7. Fluorescence microscopy study of Copper complex with HSA molecules

The fluorescence microscopy studies a valuable tool to investigate the optical waveguide properties of copper complex-HSA micro structures. The bluish green and yellowish-green micro-rods were clearly observed by using fluorescence microscopy shown in Fig. 7. Upon excitation with UV and blue light sample shows rod shaped particles with bluish green and yellowish-green luminescence respectively. In solution phase, the copper complex are entered into the HSA microparticle and possibly to be distributed randomly confirmed by luminescence property. It is thought that for the period of the development of the doped microparticles, hydrophobic and π-π interactions induces the

aggregation process of HSA and copper complex molecules into microrods [29]. The Fluorescence intensity also increases upon high dilution on HSA molecules. The uniform microrods exhibited yellowish-green emission with very bright luminescence spots at both tips and comparatively weaker emission from the bodies of the rods, which is an important feature of an optical waveguide property. This optical property also allied to the single-crystalline character and the strong fluorescence emission activities of the copper complex-HSA microrods.

3.8. Antibacterial activity

The *in vitro* biological properties of the complex were tested against pathogenic bacteria by the agar disc diffusion method. In Fig. 8, the minimum inhibitory concentration (MIC) values of the compounds are briefly described. A relative study of the DMAP and its complex (MIC values) indicates that complex demonstrate higher antimicrobial activity than the free DMAP [30]. The increased activity of the metal chelates can be explained by overtone concept and the Tweedy chelation theory. According to Overtone's concept of cell permeability, the lipid membrane that surrounds the cell opens the route of only the lipid soluble materials. That lipophilicity is a vital aspect, which controls the antimicrobial activity. Due to the overlap of the DMAP orbital and partial sharing of the positive charge of the metal ion, the polarity of the metal ion will be reduced to a greater extent which increased lipophilicity [31]. Therefore the penetration of the bacterial cell membranes and blocks the metal binding sites in enzymes of microorganisms and restricts further growth of the microorganisms and as a result microorganisms die.

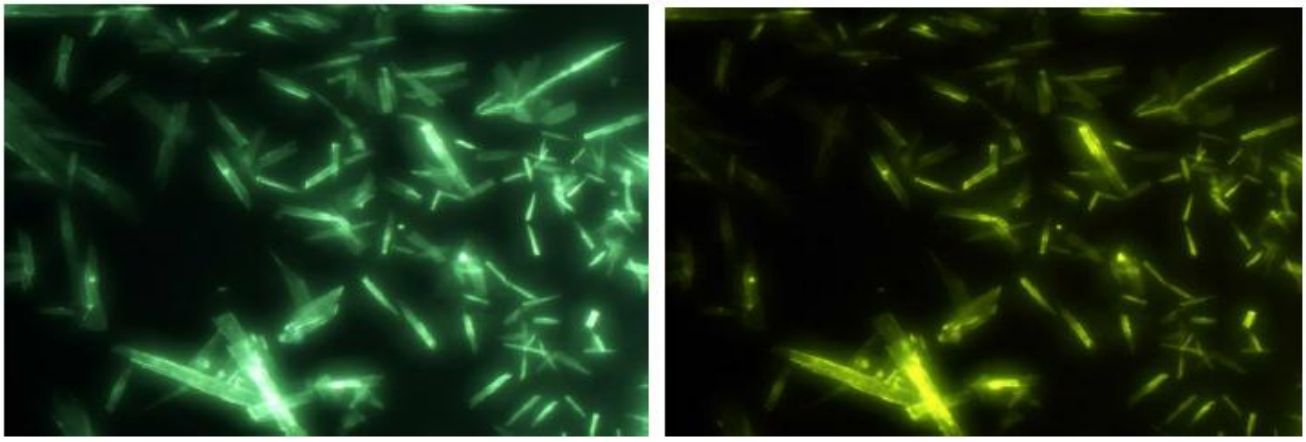

Rod shaped particles shows with bluish green and yellowish-green luminescence excitation with UV and blue light respectively.

Fig. 7: Fluorescence microscopy image of Copper complex with HSA microrods.

Fig. 8: MIC (minimum inhibitory concentration in µg/mL) values of DMAP and synthesized compound.

4. CONCLUSIONS

Synthesized square planar copper (II) complex was characterized by spectroscopic and single crystal X-ray crystallographic methods. The electronic spectrum of the compound has been interpreted by TDDFT calculations. The binding mechanisms suggested that the Cu (II) complex bind with HSA through a static quenching mechanism. Synthesis of Cu (II) complex with HSA microcrystals, which might be introduced as the building block for novel optoelectronic devices. The antibacterial screening confirmed that copper (II) complex is good biologically active.

5. ACKNOWLEDGEMENT

We gratefully acknowledge the financial support received from [Sanctioning Memo No.:620/MC/RUSA -2.0/PROJECT/19/13(12) and 620/MC/RUSA-2.0/ PROJECT/19/13(11) Dated:14.03.2019] RUSA 2.0 Component: 8 and Midnapore College (Autonomous).

Electronic supplementary information (ESI):

Crystallographic data for the structural analyses have been deposited with the Cambridge Crystallographic Data Centre, CCDC No. 1430676 for the copper compound.

6. REFERENCES

1. Mathie A, Sutton GL, Clarke CE, Veale EL. *Pharmcol Ther*, 2006; **111:**567-583.
2. Stöckel J, Safar J, Wallace AC, Cohen FE, Prusiner SB. *Biochemistry*, 1998; **37(20):**7185-7193.
3. Wu F, Wang J, Pu C, Qiao L, Jiang C. *Int. J. Mol. Sci.*, 2015; **16(3):** 6419-6431.
4. Arendsen LP, Thakar R, Sultan AH. *Clin. Microbiol. Rev.*, 2019; **32(4):**125-143.
5. Uauy R, Olivares M, Gonzalez M. *Am J Clin Nutr.*, 1998; **67(5):**952S-959S.
6. Bost M, Houdart S, Oberli M, Kalonji E, Huneau JF, Margaritis I. *J. Trace. Elem. Med. Biol.*, 2016; **35:**107-115.
7. Karlin KD, Tyeklar Z, Bioinorganic Chemistry of Copper, Chapmann & Hall, New York, 1993.
8. Hirayama K, Akashi S, Furuya M, Fukuhara KI. *Biochim Biophys Res Commun.*, 1990; **173(2):**639-646.
9. Sulkowska A. *J. Mol. Struct.*, 2002; **614:**227-232.
10. Soares S, Mateus N, Freitas VD. *J. Agri. Food Chem.*, 2007; **55(16):**6726-6735.
11. Bauernschmitt R, Ahlrichs R. *Chemical Physics Letters*, 1996; **256:**454-464.
12. Stratmann RE, Scuseria GE, Frisch MJ. *J Chem Phys.*, 1998; **109(19):**8218-8224.
13. Cossi M, Rega N, Scalmani G, Barone V. *J. Comput. Chem.*, 2003; **24(6):**669-681.
14. O'boyle NM, Tenderholt AL, Langner KM. *J. Comput. Chem.*, 2008; **29(5):**839-845.
15. Sheldrick GM. *Acta Crystalloqr A.*, 2008; **64(Pt.1):**112-122.
16. Farrugia LJ. *J. Appl. Cryst.*, 1999; **32:**837-838.
17. Wang L, Guo DG, Wang YY, Zheng CZ. *RSC Advances*, 2014; **4(102):**58895-58901.
18. Dey S, Mukherjee T, Sarkar S, Evans HS, Chattopadhyay P. *Transition Metal Chemistry*, 2011; **36(6):**631.
19. Machura B, Świtlicka A, Penkala M. *Polyhedron*, 2012; **45(1):**221-228.
20. Bhowmik P, Harms K, Chattopadhyay S. *Polyhedron*, 2013; **49(1):**113-120.
21. Pramanik AK, Sarkar D, Mondal TK. *Polyhedron*, 2015; **102:**32-40.
22. Sarker KK, Halder SS, Banerjee D, Mondal TK, Paital AR, Nanda PK, Raghavaiah P, Sinha C. *Inorganica Chimica Acta*, 2010; **363(12):**2955-2964.
23. Patra A, Sen B, Sarkar S, Pandey A, Zangrando E, Chattopadhyay P. *Polyhedron*, 2013; **51:**156-163.
24. Benesi HA, Hildebrand JH. *J. Am. Chem. Soc.*, 1949; **71(8):**2703-2707.
25. Jhonsi MA, Kathiravan A, Renganathan R. *Colloids Surf. B*, 2009; **72(2):**167-172.
26. Stern O, Volmer M. *Z. Phys.*, 1919; **20:** 183-187.
27. Ahmad B, Parveen S, Khan RH. *Biomacromolecules*, 2006; **7(4):**1350-1356.
28. Kathiravan A, Renganathan R. *Polyhedron*, 2009; **28(7):**1374-1378.
29. Chen W, Peng Q, Li Y. *Cryst. Growth Des.*, 2008; **8(2):**564-567.
30. Sheikh J, Juneja H, Ingle V, Ali P, Hadda TB. *J. Saudi Chem. Soc.*, 2013; **17(3):**269-276.
31. Prakash CR, Raja S. *J. Saudi Chem. Soc.*, 2013; **17:**337-344.